Latin American Journal of Solids and Structures
www.lajss.org

Numerical study of confinement in short concrete filled steel tube columns

Abstract

This study presents a numerical investigation into the behaviour of short concrete filled steel tubular (CFST) columns. Three Dimensional Nonlinear finite element analysis of the compression process is performed using commercial software ABAQUS v6.9 (2009). Steel tubes of different geometries and in-filled with different grades of concrete are chosen for modelling from literature. The proposed FE model is validated by comparing its results with those of the corresponding experimental specimens. The model is further used to study the variation of radial confining pressure f_{cp} provided by the steel tube to the concrete core. It is observed that the value of f_{cp} varies widely throughout the length of the CFST, with the values in the area adjacent to top and bottom platens being markedly higher than the values in-between due to the end restraint provided by the machine platens. This is in contrast to the present confined concrete model which uses a uniform value of confining pressure throughout the height. Effect of effective length of column and interfacial friction present between the platen and specimen are found to be negligible on behaviour of short CFST column.

Keywords

Concrete filled steel tubes; ABAQUS; finite element; axial compression; nonlinear analysis; radial confining pressure; concrete; composite columns; circular hollow sections

P.K. Gupta*
Heaven Singh

Department of Civil Engineering,
Indian Institute of Technology
Roorkee, INDIA
* Corresponding author email:
spramod_3@yahoo.com, Phone No.
+911332-285425

1 INTRODUCTION

Concrete filled steel tubular (CFST) columns are a form of composite construction that comprise concrete filled into a steel tube, with the advantages of both materials combined into one. The steel tube provides lateral confinement to the concrete core which results in an increased concrete compressive strength and deformation capacity. The concrete infill, in return, prevents the inward local buckling in steel tubes. The axial load bearing capacity of CFST short columns is thus higher than the summation of axial load-bearing capacities of the concrete core and the corresponding hollow steel tube. The placement of the stiffer steel tube at the periphery of concrete core also enhances moment of inertia of the member. This provides many structural advantages such as improved flexural resistance and higher initial stiffness. The steel tube also acts as the formwork for construction and supports the initial construction loads, thus reducing the overall cost (Shanmugam and Lakshmi 2007).

CFST columns have been a major area of study among the researchers since late 1990s. A detailed study by Tomii et al. (1977) on 268 CFST columns highlighted that two failure modes could be observed during the test, namely overall buckling for slender columns and the crushing of concrete accompanied by local buckling of steel tube for short columns. Additionally, the post-yield behaviour of circular and octagonal CFST columns was found to exhibit strain hardening or perfectly plastic behaviour. But for square CFST columns, strain softening was the failure mode observed

after the peak load was reached. Johansson and Gylltoft (2001) investigated the behaviour of stub CFST columns when both steel and concrete were axially loaded, as well as when only concrete or only steel was loaded. They concluded that the in either loading pattern, concrete strength was augmented due to the bond between steel and concrete. Due to the bond between concrete and steel, all of the stub columns sustained large deformations with almost completely maintained load resistance. O'Shea and Bridge (2000) also tried to estimate the strength of CFST columns under different types of loadings. The loadings were purely axial as well as with small eccentricity. The load was applied through loading the steel only, concrete only, and steel and concrete simultaneously. All the tested specimens were short with a length/diameter ratio of 3.5. They concluded that the degree of the confinement was highest when only the concrete was loaded axially and the thin-walled steel was used as pure circumferential restraint. Schneider (1998) tested fourteen specimens to study the effect of tube shape and steel tube thickness on the composite column strength. It was observed that circular columns provided much more post-yield axial ductility than square or rectangular columns. This was attributed to the same level of confinement along the entire cross section in circular sections, while in rectangular shapes maximum confining stress occurs at corners (owing to stress concentration) and reduces towards the centre of the cross section. Huang et al. (2002) tested seventeen concrete-filled steel tube column specimens but with a higher column diameter-to-thickness ratio (D/t). They also concluded that circular columns provided better post-peak ductility even for high D/t ratios up to 150. Sakino et al (2004) also investigated the behaviour of stub columns loaded under compression. One hundred fourteen specimens of different cross sectional shapes and varying width to thickness ratios were tested. Normal strength concrete as well as high strength concrete was used as in-fill. Giakoumelis and Lam (2004) tested fifteen circular specimens to examine the effect of bond strength between concrete and steel tube on the behaviour of CFST columns. The specimens were tested with inside walls of the hollow tube greased to minimize its bond with concrete as well as in non-greased condition. It was found that the effects of the bond between the concrete and the steel tube is more critical for high-strength concrete while for normal strength concrete, the reduction in the axial capacity due to the loss of bonding between steel and concrete was negligible. Gupta et al. (2007) tested 12 stub columns and concluded that for smaller D/t ratio, steel tube provides better confinement to concrete. A two-dimensional nonlinear computational model was also developed for the CFST specimens on the commercial finite element code ANSYS 8.0. Oliveira et al. (2009) also tested 32 CFST members in axial compression. All these samples had a steel tube of outer diameter 114.3 mm and wall thickness 3.35 mm. Four different L/D values, viz. 3, 5, 7 & 10 were used in conjunction with 4 different grades of concrete having 30, 60, 80 and 100 MPa as nominal compressive strength. It was observed that short columns (L/D = 3) filled with normal strength concrete generally collapsed a strain hardening behaviour due to the confinement offered by steel tube. The inherent brittleness of high strength concrete tends to cancel out due to the confinement offered by steel tube; therefore a gradual strain softening was observed for steel tubes filled with 80 MPa and 100 MPa grade concrete. Ellobody et al (2006) modelled various circular CFST columns from literature using ABAQUS 6.3 code and obtained a good agreement between experimental and simulated results. Bahrami et al. (2013) also simulated behaviour of axially loaded stiffened concrete filled steel composite stub columns using the FE code LUSAS. The authors reported that the columns failed due to concrete crushing about their mid-height where the steel wall locally buckled. The effect of end friction between deforming tube and compressing platen interfaces for hollow aluminum tubes was studied by Gupta and Gupta (2005). They found that for hollow aluminum pedestal the end friction may change mode of deformation without appreciable change in load-deformation history.

The aim of this investigation is to utilize the general purpose finite element program ABAQUS to perform nonlinear numerical simulations of short concrete filled steel tubular columns (CFST) subjected to axial compressive loads. The proposed computational model is then validated against the experimental data available in literature from Giakoumelis and Lam (2004); Gupta et al. (2007);

Sakino et al. (2004); Schneider (1998) and Oliveira et al. (2009).Thereafter the developed model is utilized to study the variation of confining pressure along the length of CFST column. The variation of confinement of concrete core has not been reported in any of the available literature to the best of the knowledge of the authors. Furthermore, the influence of diameter/thickness (D/t) values (while keeping diameter constant) on energy absorption capacity of CFST specimens is also studied. In a typical frame the load is transferred to the column from the beams through the beam-column joint. The behaviour of the column
may vary with the change in geometrical dimensions of the load transferring beams. This change in geometrical dimensions of beams results change in effective length of supporting column. The change in behaviour of the column may be modeled by taking different effective length of column. This aspect has been studied and reported by considering various lengths of a column. Effect of friction present between the platen and column specimen on the behaviour of the column is also investigated and re-ported.

2 NUMERICAL MODELLING METHOD

2.1 General

Numerical study of any experimental problem affords a researcher complete freedom to explore in detail any number of factors influencing that phenomenon. Thus following the increased use of CFST columns in practical applications, many numerical models are being proposed to simulate the response of such members. As observed from the available literature, the failure modes of short concrete-filled steel tubular columns under axial compressive loads are characterized by yielding of the hollow sections and concrete crushing. Suitable constitutive models must be adopted for concrete and steel tube to capture the mode of deformation of CFST columns.

2.2 Model description

2.2.1 Meshing

In any finite element based analysis, selection of the appropriate element type is instrumental to the success of the computational procedure. The Abaqus Standard module inset in ABAQUS 6.9 (2009) is used for modelling. The Abaqus Standard module consists of a comprehensive element library that provides different types of elements catering to different situations.

When a CFST column is subjected to axial compression, the in-filled concrete core behaves as a single solid block that undergoes compression without any rotation. Abaqus (ABAQUS 6.9, 2009) provides a set of Solid (continuum) elements specially designed for such cases. The most commonly used elements are 4-node linear tetrahedron (C3D4), 6-node linear triangular prism (C3D8) and 8-node linear brick elements (C3D8) [12]. Each of these elements possesses three translational degrees of freedom (DOFs) at each node. It is observed that for CFST members, C3D4 and C3D6 elements provide slow convergence and require very fine mesh which increases computational time and effort. C3D8 brick elements are found to be most suited from both the accuracy as well as time required viewpoints. It can be used for complex nonlinear analysis involving contact, plasticity and large deformations.

The hollow steel tube can be meshed by using either the shell elements or the solid brick elements. However, in addition to the translational DOFs, the shell elements also possess rotational DOFs. This may give rise to compatibility issues at the junction of concrete core and steel tube, since the concrete core elements come with only translational DOFs. Hence, trials were performed using C3D8 elements to mesh the steel tube also. A single layer of these elements through the element thickness is found to reproduce the deformed shape of the tube with good accuracy.

The assembly of concrete core and the steel tube is confined by rigid plates, one each at the top and the bottom. The rigid plates are defined using the Discrete Rigid option available in Abaqus (ABAQUS 6.9, 2009). The plates are meshed by the elements available in the rigid element library.

Due care was taken to ensure that the meshing of concrete core and hollow tube is finer as compared to that of rigid plates; if not so, the column assembly will tend to penetrate into the rigid plate. Surface to surface contact is provided between the faces of the column in contact with the top and the bottom plates. The rigid part must always be the master surface. The value of coefficient of friction is kept as 0.1 at both ends.

2.2.2 Material Modelling

(a) **Steel tube**: An elastic-perfectly plastic model is used to model the behaviour of steel tube. The Young's modulus and Poisson ratio of the material are taken as 200 GPa and 0.3 respectively. Von-Mises yield criterion is used to define the yield surface for steel. Once the stress in steel reaches yield surface, it carries no further loading and becomes perfectly plastic.

(b) **Concrete**: The Drucker Prager model provided in the Abaqus (ABAQUS 6.9, 2009) library is used for simulating the behaviour of concrete. The model is suitable for describing the response of materials with compressive strength 10 times or higher than the tensile strength. To simulate the confinement provided by steel tube to concrete, a confined stress-strain model provided by Huang et al (2002) is used for the concrete in conjunction with Drucker Prager model for plastic hardening of concrete. The behaviour of confined concrete vis-à-vis unconfined concrete is represented in Fig. 1

The graph for confined concrete is linear elastic up to $0.5f_{cc}$; it is described using the initial modulus of elasticity E_c and the Poisson's ratio, which is taken as 0.2. The formulas and other mathematical details of the model are illustrated in Huang et al. (2002).

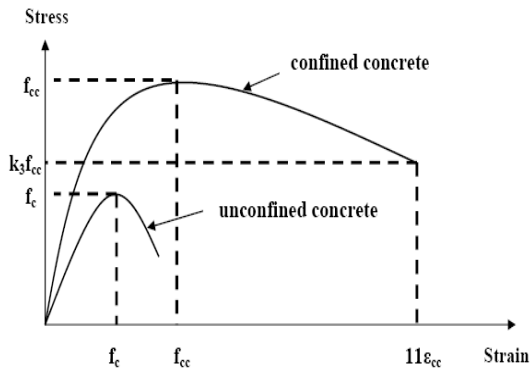

Figure 1: Model for confined concrete vis-à-vis unconfined concrete.

2.2.3 Interface Modelling

In order to obtain all the above mentioned advantages from the CFST columns, it is pertinent that steel tube and concrete core composite must behave as a single member and not merely as a combination of two different materials. This makes the simulation of composite action between concrete and steel tube the single most important factor guiding the behaviour of the composite member. The normal contact between the two materials is provided using friction, with the inner surface of the steel tube as the slave surface. The coefficient of friction between the two surfaces is chosen as 0.25. Hard Contact is provided between the two surfaces, which causes the pressure to be transmitted across the two surfaces only when there is actual contact among them, while causing the surfaces to separate under the influence of a tensile force.

2.2.4 Loading and boundary conditions

The steel tube and the concrete core are left completely unrestrained in all directions to allow any possible deformation in the column. The bottom rigid plate is fixed completely using the encastre

boundary condition applied at its reference node, while the loading was applied by providing total displacement in small increments at the top rigid plate (to simulate the actual strain controlled test conditions). The value of the total displacement was generally kept slightly higher than the maximum value for the same in the corresponding experimental investigation.

3 VALIDATION OF PROPOSED MODEL

The precision of the numerical model was judged by comparing the results from the model against the experimental results of authors like Giakoumelis and Lam (2004); Gupta et al (2007); Sakino et al (2004); Schneider (1998) and Oliveira et al (2009). The parameters under evaluation were the a) peak compressive load capacity b) load vs. displacement response at the moving end c) deformed shape of the column. The following paragraphs present the results obtained with the computational model for the experimental studies (see Table 1) carried out by the mentioned researchers and available in literature

Column	Source	Outer diameter D (mm)	Wall thickness t (mm)	D/t	L/D	Steel yield strength f_y (MPa)	Concrete comp. strength f_c (MPa)	Experimental load capacity P_{exp} (KN)	Simulated load capacity P_{sim} (KN)	P_{sim}/P_{exp}
C-30-3D	Oliveira et al.	114.3	3.35	34.12	3.0	287.33	32.7	737.0	763.40	1.036
C-60-3D	Oliveira et al.	114.3	3.35	34.12	3.0	287.33	58.7	952.0	971.32	1.020
C-80-3D	Oliveira et al.	114.3	3.35	34.12	3.0	287.33	88.8	1136.2	1173.62	1.033
C-100-3D	Oliveira et al.	114.3	3.35	34.12	3.0	287.33	105.5	1453.1	1313.80	0.904
C3	Giakoumelis and Lam	114.43	3.98	28.75	2.62	343	31.4	993.86	1029.43	0.965
C8	Giakoumelis and Lam	115.04	4.92	23.38	2.61	365	104.9	1787.0	1708.66	0.956
C14	Giakoumelis and Lam	114.54	3.84	29.82	2.61	343	98.9	1359.0	1425.17	1.048
CC4-A-4-1	Sakino et al.	149.0	2.96	50.34	3.0	308	40.5	1064.0	1078.92	1.014
CC4-C-4-1	Sakino et al.	300.0	2.96	101.4	3.0	279	41.1	3277.0	3333.78	1.017
CC4-D-4-1	Sakino et al.	450.0	2.96	152.0	3.0	279	41.1	6870.0	6751.75	0.983
D4M3F1	Gupta et al.	112.56	2.89	38.95	3.0	360	28.88	650.0	657.97	1.012
D4M4F1	Gupta et al.	112.56	2.89	38.95	3.0	360	36.67	764.15	758.10	0.992
C1	Schneider	140.8	3.0	46.93	4.3	285	28.18	881.0	875.0	0.993
C3	Schneider	140.0	6.68	20.96	4.4	537	28.18	2715.0	2637.32	0.971
Mean										**0.996**
Std. Dev.										**0.0384**

Table 1: Material properties and results of simulated specimens

Oliveira et al. (2009) tested sixteen specimens with different grades of infill and different length to diameter (L/D) ratios. Four specimens filled with different grades of concrete and L/D=3 were simulated. Table 1 shows the details of the specimens and a comparison between the experiment and simulated load capacities. Figure 2 represents the experimental results versus results from the proposed model. From the figures, it is evident that a good reproduction of the load deformation pattern can be obtained from the model.

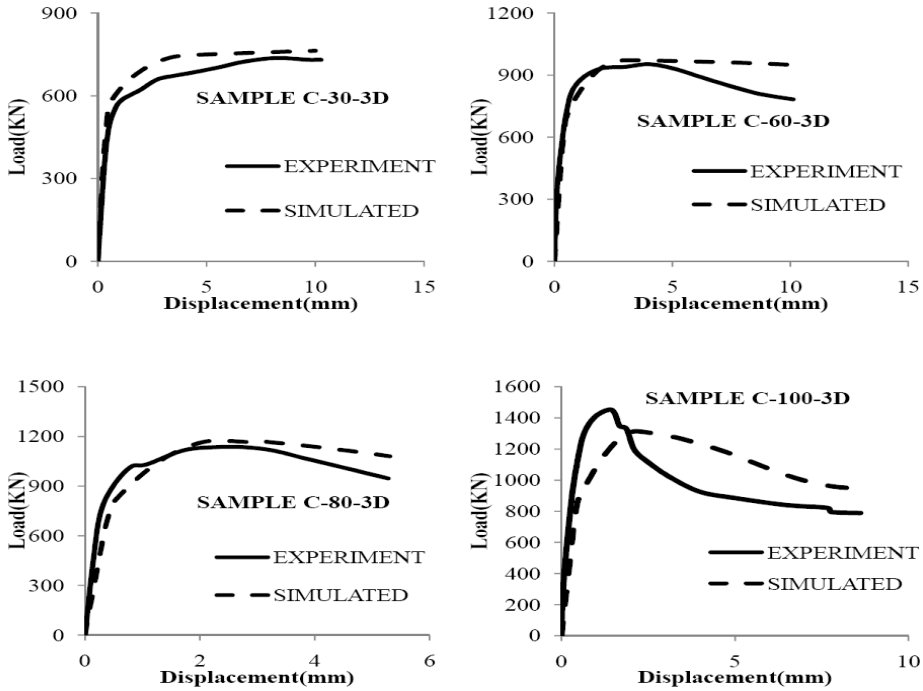

Figure 2: Experimental results of Oliveira et al. vs results of numerical model

15 specimens were tested by Giakoumelis and Lam (2004) to study the effect of bond strength on response of CFST. Two non-greased specimens C3 and C8 were simulated using the proposed model. The details of the specimens are provided in Table 1. From Figure 3, the experimental and the numerically obtained deformed shapes are observed to be in good agreement. The computational model is able to replicate the experimentally observed local buckling of steel tube wall. Figure 4 represents the experimental results versus results from the proposed model. The model follows the experimental load-deflection behaviour of the specimens closely. Figure 5 shows the experimental vs. simulated load-deformation response for sample C8.

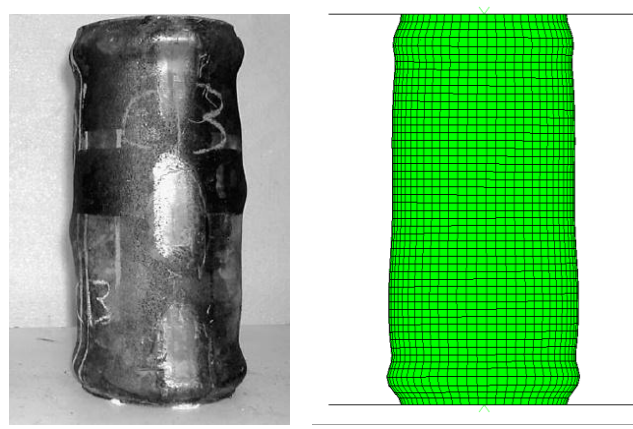

Figure 3: Comparison of experimental and simulated deflected shape of Giakoumelis and Lam Specimen C3

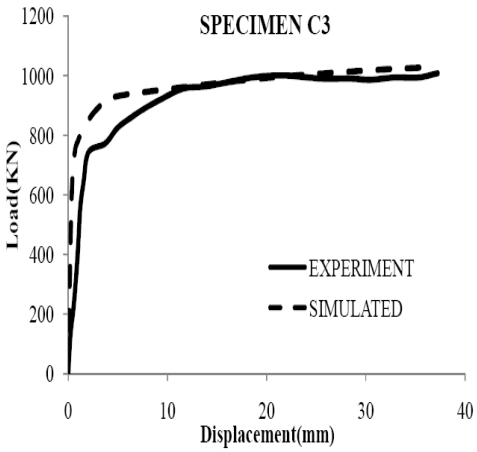

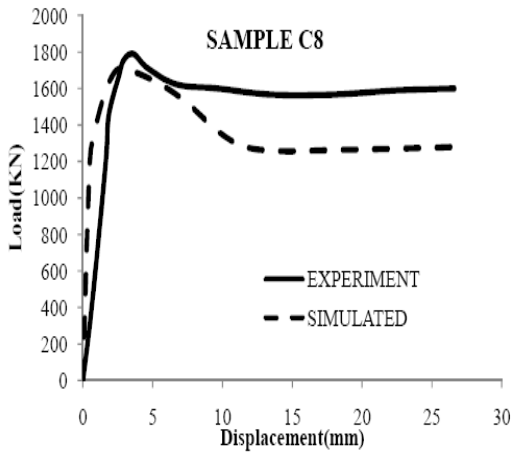

Figure 4: Experimental vs numerical model results of Giakoumelis and Lam Sample C3

Figure 5: Experimental vs numerical model results of Giakoumelis and Lam Sample C8

Sakino et al. (2004) tested 114 specimens of different shapes and in-filled with different grades of concrete. In the present study, three of his specimens are simulated using the computational model. All the specimens were of L/D ratio 3. The details of the specimen and comparison of peak compressive load capacity are presented in Table 1. Figures 6 through 8 present a graphical comparison of load-deformation behaviour of the specimens.

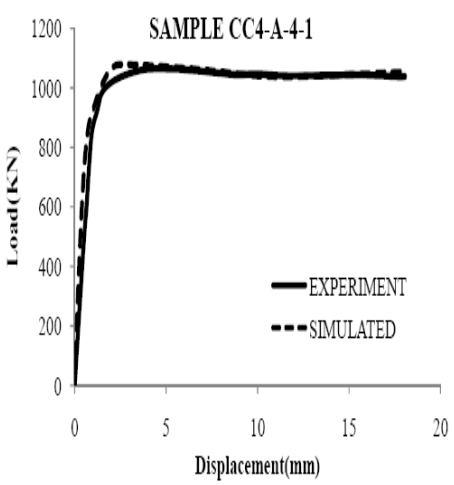

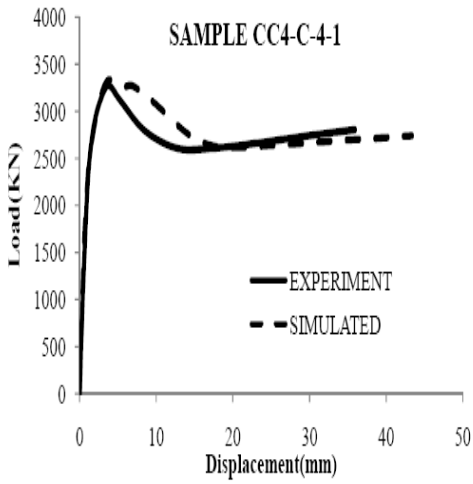

Figure 6: Experimental vs numerical model results of Sakino et al. Sample CC4-A-4-1

Figure 7: Experimental vs numerical model results of Sakino et al. Sample CC4-C-4-1

Gupta et al (2007) tested 72 CFST columns ranging from slender columns with L/D= 7.2 to stub columns with L/D=3. Two of the specimens D3M4F1 and D4M4F1, both filled with M40 grade of concrete were modelled. Figure 9 shows the load-displacement curve for specimen D4M4F1. Figure 10 presents a comparison of load-deflection behaviour between experiment and simulated results for

the sample D4M3F1. It is evident that the proposed model closely predicts the peak compressive load values for both the samples simulated

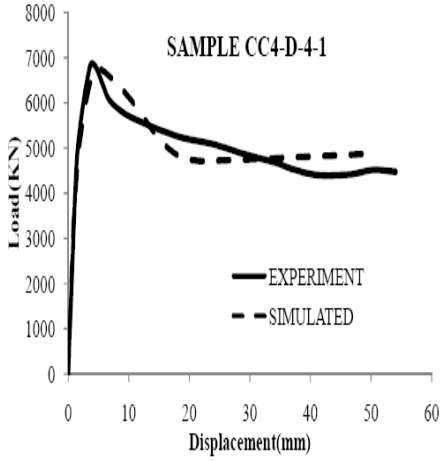

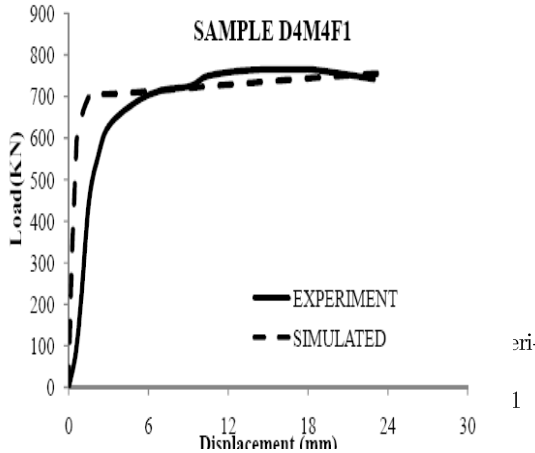

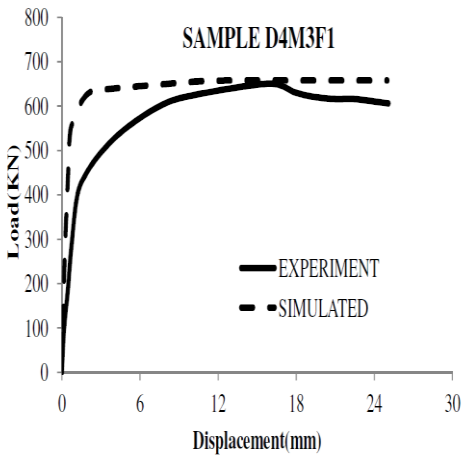

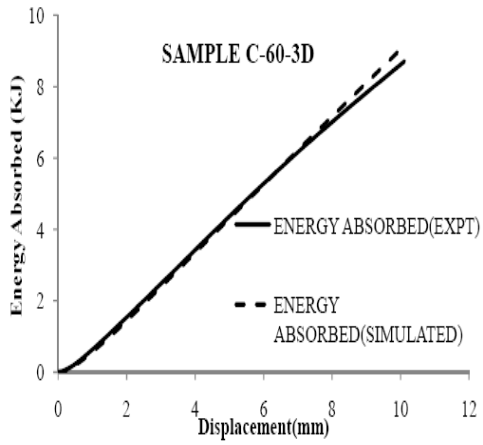

3.1 Effect of End Friction

It is well known that in an actual framed structure, the compression members do not carry load in isolation; rather, they are a part of a network of a continuous framework of beams and columns, designed so as to provide a well-defined load transfer path. The presence of beams often causes a certain degree of fixity (and hence lateral restraint) near the top and bottom ends of columns. Gupta and Gupta (2005) studied the effect of end friction between tube-platen interfaces for hollow aluminum tubes. It was observed that the friction affects the mode of deformation to a great extent. In the CFST modeling explained above, a friction coefficient of 0.15 was used at both column ends to provide the fixity. However, in actual structures, the effect of presence of beams at column ends may be far more significant. To evaluate this effect, the authors simulated two specimens viz. CC4-A-4-1 (Sakino et al., 2004) and C3 (Giakoumelis and Lam, 2004) with different coefficients of friction (f), ranging from very low (f=0.025) to very high (f=0.5) end joint rigidity. The results of these simulations are presented in Figures 12 and 13. The peak axial load values are tabulated in Table 2. As a simplified notation, the end frictions are denoted as friction at top (f_{top}) / friction at bottom (f_{bot}). Therefore 0.25/0.15 implies a top end friction of 0.25 and a bottom end friction of 0.15. If both end frictions are equal, only a single value of variable 'f' is mentioned.

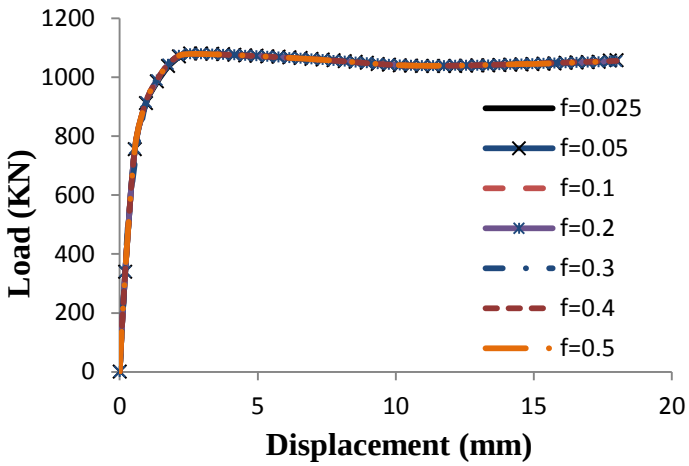

Figure 12: Effect of different end friction values of loadties of samples
deformation behaviour of Sakino et al. Sample CC4-A-4-1

Column →	CC4-A-4-1 (Sakino)	C3 (Lam)
f ↓	P_{sim} (KN)	P_{sim} (KN)
0.025	1078.97	-
0.05	1079.14	1028.65
0.1	1078.90	1029.75
0.15 (from Table 1)	1078.92	1029.43
0.2	1078.79	1029.51
0.3	1078.85	1028.96
0.4	1078.70	1030.46
0.5	1078.68	1031.63
0.25/0.15	-	1028.87
0.5/0.4	-	1027.44

Table 2: Peak axial load capaciat different end frictions

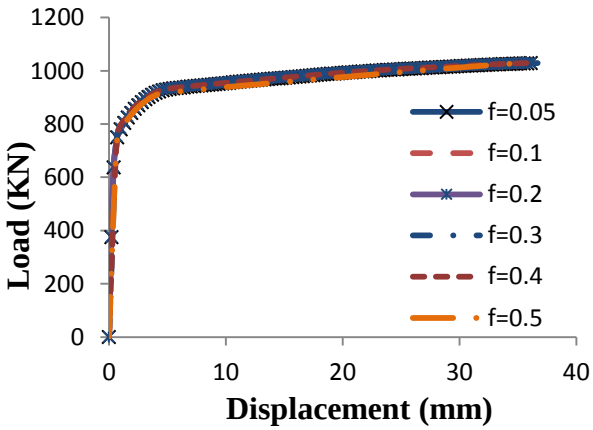

Figure 13: Effect of different end friction values of loadfrictions
deformation behaviour of Giakoumelis and Lam Sample C3

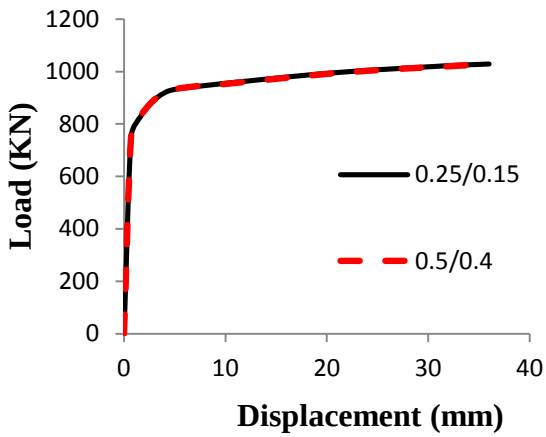

Figure 14: Effect of different end
for Sample C3

It is quite evident from Figures 12 to 13 that the load-deflection response of a CFST column is unaffected by the friction between CFST column ends and surrounding beams. Further, the peak load values in Table 2 are also almost identical for different end frictions for a given sample.

The effect of end friction values on the deformed shape of columns was also examined. Figs. 15 a) and b) show deflected shape of column C3 (Giakoumelis and Lam, 2004) for slarge (f=0.4) and ends-different (0.25/0.15) friction values. Comparing these figures with each other and Figure 5 (f=0.15), it becomes clear that the local buckling pattern of stub CFST column is independent of the end friction.

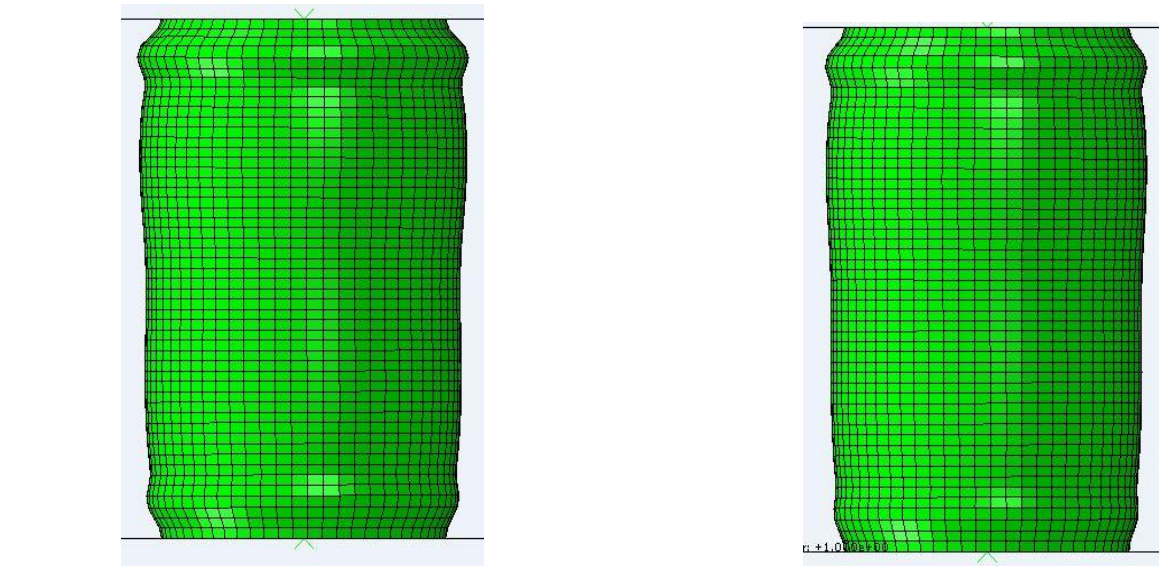

a) b)

Figure 15: Deformed shape of Sample C3 at a) f=0.4 at both ends b) f=0.25 at top end and 0.15 at bottom end

The deformed shapes in Figs. 15 a) and b) show a good resemblance to the experimental deformed shape (see Figure 5) also.

3.2 Study of Effective Length

In a framed structure, the relative displacement of the ends of the column may be restrained due to beams at either ends. Therefore, the effective length of the column (L_{eff}, which actually undergoes deformation) may be lower than its end-to-end unsupported length L (Clause 25.2, ANNEX E, IS 456:2000). Hence, in the present study, simulations were performed for different effective lengths of columns. Four typical columns of Sakino CC4-A-4-1 configuration (Sakino et al., 2004) of effective length (L_{eff}) 0.9L, 0.85L, 0.8L and 0.75L were analyzed. The load-deformation response for these members were plotted with respect to different α (= L_{eff}/L). Figure 16 shows the behaviour of these columns on a single graph. The peak load-carrying capacity of the respective columns is shown in Table 3.From Figure 16, it is evident the change in effective length of a CFST column does not affect the characteristic response of the column. Thus, the presence of flexural members does not alter much the behaviour of surrounding CFST members loaded in axial compression.

4 STRAIN ENERGY

The proposed model was further used to compare the experimental strain energies with the corresponding values for the same obtained from Abaqus (ABAQUS 6.9, 2009). While the experimental strain energy E_{exp} was calculated as the area under the experimental load-displacement curve, the corresponding values from modelling were labelled as simulated strain energy E_{sim}. Table 3 presents a comparison of numerical values of both these variables for all the simulated samples. Further, Figures 17 through 19 graphically illustrate the experimental strain vis-a-vis simulated values for selected specimens. The tabular and graphical data presented here clearly indicate that the numerical model is able to predict the values of strain energy for the specimens very closely at any stage of loading.

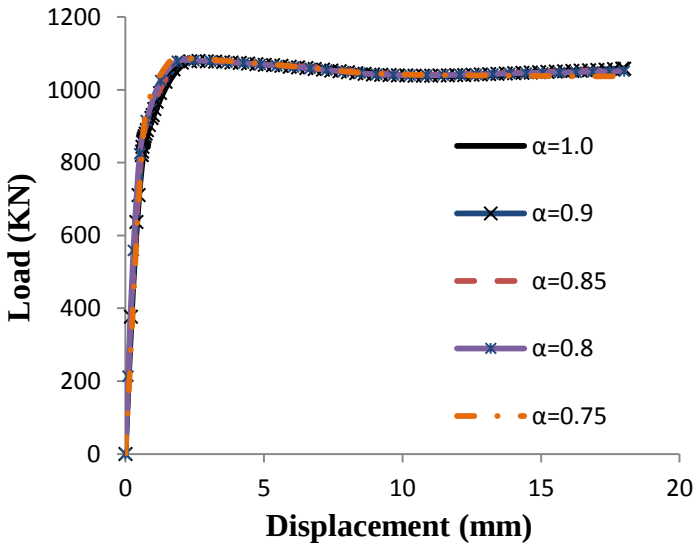

Figure 16: Load- deformation behaviour of Sample CC4-A-4-1 at different effective lengths

$\alpha(=L_{eff}/L)\downarrow$	P_{sim} (KN)
1.0(from Table 1)	1078.92
0.9	1079.02
0.85	1078.83
0.8	1078.70
0.75	1078.79

Table 3: Peak axial load capacities of sample at different effective lengths

From Table 4, it is observed from Sakino samples (CC4-A-4-1 through CC4-C-4-1) that as D/t is increased (keeping thickness constant while diameter of sample is increased), the energy absorption of the sample increases. This is due to the increase in area of concrete as the sample size increases. However, owing to the lack of the data (in the present study) for the converse, i.e. what will be the effect of D/t when thickness is changed while keeping diameter constant, a small numerical study was carried out on specimen CC4-A-4-1 by creating 3 virtual specimens CC4-A-4-1-V1 through CC4-A-4-1-V3 having D/t ratio of 25, 75 and 100 respectively; the original specimen (D/t=50) was labelled CC4-A-4-1-O. The results of this study are tabulated in Table 5, where it can be clearly seen that the energy absorption at any stage decreases as the thickness of steel tube decreases for the same tube diameter. Further, owing to the increase in concrete area with decreasing steel tube thickness, the energy absorbed by concrete increases; the energy absorbed by steel correspondingly reduces due to the reduction in steel area. The values for both are shown in Table 5 and are observed to be varying parabolically with D/t ratio.

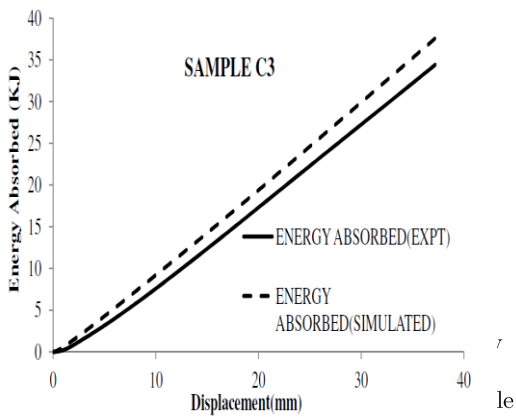

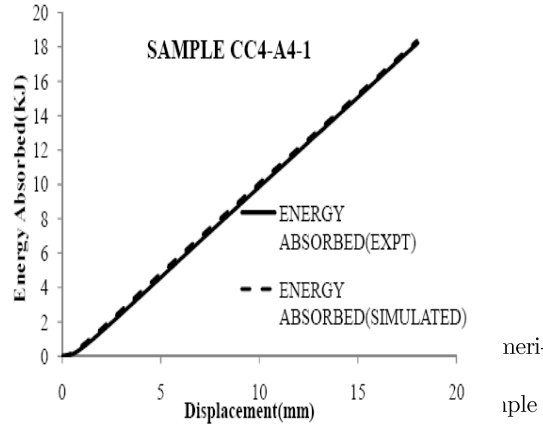

cal en neri-

le C3 ıple

CC4-A-4-1

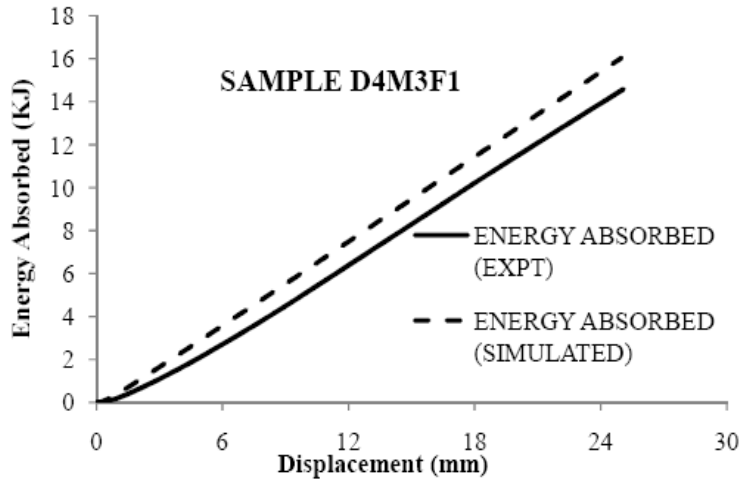

Figure M3F1

Column	Source	Outer diameter D (mm)	D/t	Experimental energy absorbed E_{exp} (KJ)	Simulated energy absorbed E_{sim} (KJ)	E_{sim} / E_{exp}
C-30-3D	Oliveira et al	114.3	34.12	6.811	7.109	1.044
C-60-3D	Oliveira et al	114.3	34.12	8.706	9.182	1.055
C-80-3D	Oliveira et al	114.3	34.12	5.374	5.524	1.028
C-100-3D	Oliveira et al	114.3	34.12	12.174	12.040	0.989
C3	Giakoumelis and Lam	114.43	28.75	34.400	37.673	1.095
C8	Giakoumelis and Lam	115.04	23.38	40.900	36.007	0.880
C14	Giakoumelis and Lam	114.54	29.82	18.243	18.349	1.006
CC4-A-4-1	Sakino et al	149.0	50.34	97.255	98.500	1.013
CC4-C-4-1	Sakino et al	300.0	101.35	269.513	250.320	0.929
CC4-D-4-1	Sakino et al	450.0	152.02	14.650	15.276	1.043
D4M3F1	Gupta et al	112.56	38.948	15.820	16.212	1.025
D4M4F1	Gupta et al	112.56	38.948	6.811	7.109	1.044
Mean						**1.009**
Std. Dev.						**0.060**

Table 4: Energy absorbed by various specimens

Sample	Outer diameter D (mm)	Wall thickness t (mm)	D/t	Energy Absorbed at 18 mm Disp. E_{18} (KJ)	Area of Concrete A_c (mm^2)	Area of Steel A_s (mm^2)	%age of energy absorbed by	
							Concrete	**Steel**
CC4-A4-1-V1	149	5.96	25	31.025	14750.88	2676.91	84.64	15.36
CC4-A4-1-O	149	2.96	50.34	18.243	16070.43	1357.35	92.21	7.79
CC4-A4-1-V2	149	2.00	74.5	13.267	16504.63	923.16	94.70	5.30
CC4-A4-1-V3	149	1.49	100	12.338	16737.64	690.14	96.04	3.96

Table 5: Variation of energy with D/t ratio

5 CONFINING PRESSURE STUDIES

The CFST members owe their unique properties to the radial confining pressure (f_{cp}) exerted by the steel tube on the concrete, which enhances the compressive strength and ductility of concrete. Estimating the correct value of this parameter is pivotal to finding the load resistance of CFST member under any given type of loading. However, the experimental measurement of the value of confining pressure at any section is very difficult and requires sophisticated equipment. Hence, the FEM model has been used to study its variation along the height and the circumference of the specimen.

To understand this further, the example of Sakino sample CC4-A4-1 has been taken. Assume that Z is the distance of the section considered from the top surface of the CFST member. The estimation of the radial pressure at any cross-section requires defining a circumferential path at that section. Figs. 20a) and 20b) show the cross-section under consideration (at 70 mm from top surface of CFST) and the circumferential path at that cross-section in sample CC4-A-4-1. Fig. 21 shows the confining pressure distribution for the path shown in Fig. 20b). The negative value of the confining pr. implies a compressive confining pressure on concrete.

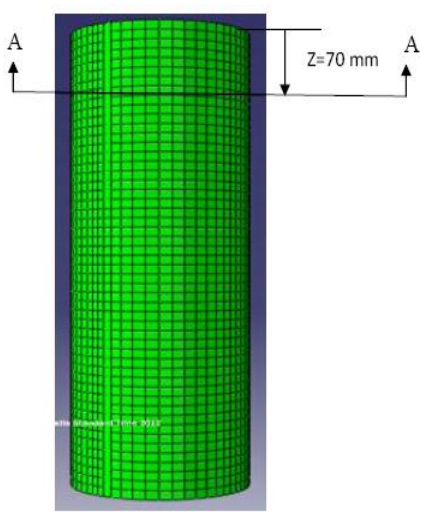

Figure 20a): A section AA cut in CFST defined in Sakino -

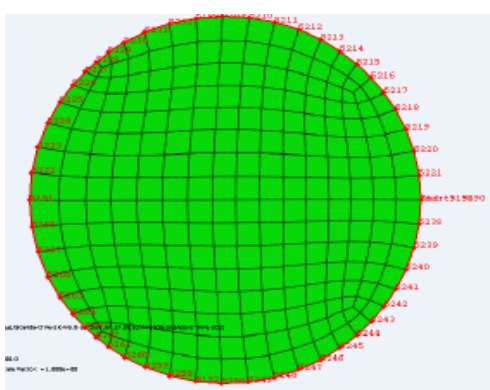

Figure 20b): A circumferential path de-

at 70 mm from top CC4-A-4-1 at 70 mm from top

It is expected that since in axial compression, concrete expands laterally in all directions, the confining pressure should be nearly constant at all points of any particular cross section in concrete. This is evident from Fig. 21, where it is observed that at any section (i.e. any Z- value), the radial confining pressure is more or less constant throughout the path.

Figure 22 presents the distribution of confining pressure at different lengths from the top (Z-values) along the circumference of the column.

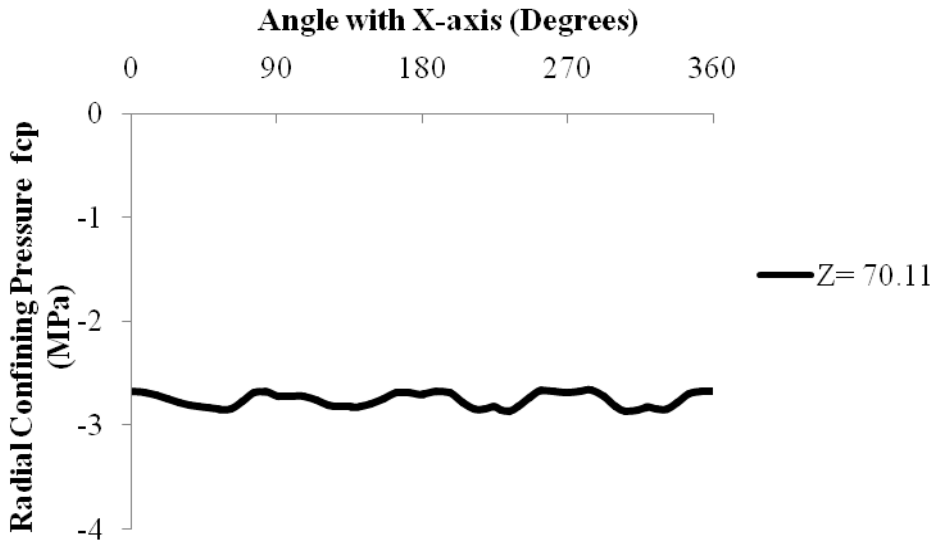

Figure 21: Radial confining pressure distribution along the circumference (at a cross-section 70 mm from top in Sakino CC4-A-4-1)

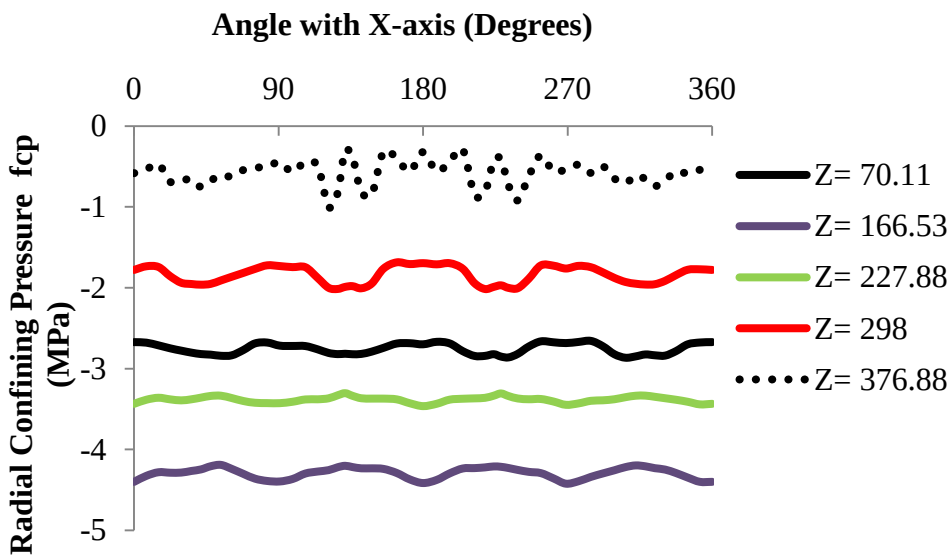

Figure 22: Radial confining pressure distribution for different sections along the height of Sakino CC4-A-4-1

From Table 1, it is noted that the length of specimen CC4-A-4-1 was 447 mm. However, Fig. 22 does not report the values of f_{cp} for the region immediately adjacent to top and bottom machine platens. This query can be answered using Figure 23, which is in fact complimentary to Fig. 22. Figure 23 represents the variation of Confining Pressure along a vertical line through the full length of the sample.

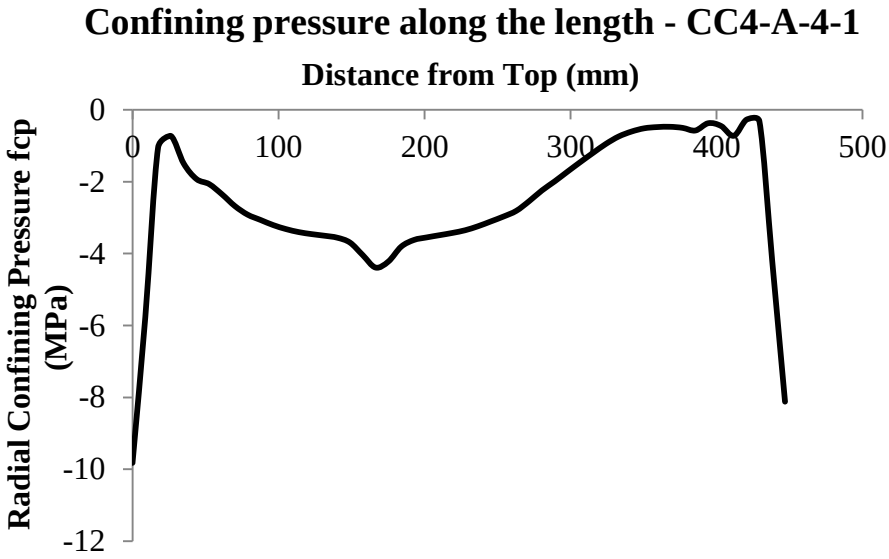

Figure 23: Variation of Confining Pressure along the height of sample Sakino CC4- A-4-1

Figure 23 is plotted by tabulating the confining pressure along any vertical line on the sample (since confining pressure at all points on any horizontal cross section is appoximately same, any vertical can be chosen). From this Fig., two interesting features can be observed:

1 It can be observed that the confining pressure in the areas adjacent to top and bottom of machine platens is much higher than the corresponding values in the remaining length of the specimen. The length of these regions was found to be between 30-50 mm for the specimens considered in this study. This can be attributed to the strong effect of end restraint caused by platen on the CFST sample. Further, it was also observed that at any cross section in these regions, the end friction may cause even the confining pressure on the same cross-section to fluctuate wildly (instead of being appoximately same), as shown in Figure 24 for sample Lam C3 (at Z=247.06, i.e. approx. 50 mm from bottom in a total specimen length of 300 mm).

2 The confined stress strain model adopted by Huang et al (2002) assumes a uniform value of lateral confining pressure f_l for the specimens, provided as:

$$\begin{aligned} f_l/f_y &= 0.043646\text{-}0.000832(D/t) \quad (21.7 \le D/t \le 47) \\ f_l/f_y &= 0.006241\text{-}0.0000357(D/t) \quad (47 \le D/t \le 150) \end{aligned} \tag{1}$$

However, Figure 23 clearly shows that the value of confining pressure varies significantly with height of the specimen even in the middle region free from end friction effect of machine platen.

Variations in Confining Pressure along the circumfrence and the length for some more specimens are Figures 24 through 27.

It is clear from Figs. 23, 25 and 27 that as we move farther away from top (or bottom) to the central portion of the CFST member, the confining pressure generally adopts a V-shape distribution, with the maximum value being attained at the region of steel local buckling in this length.

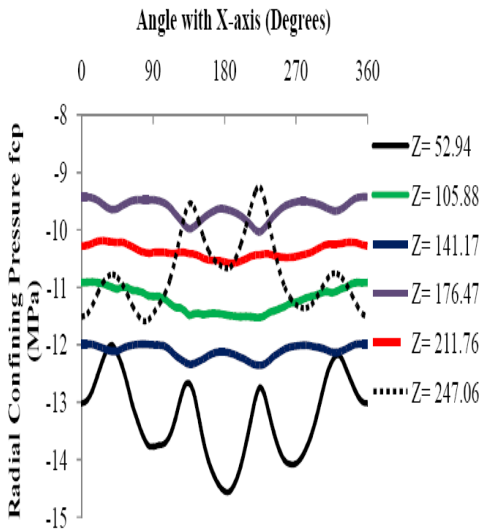

Figure 24: Radial confining pressure distribution the height of at different sections along the length of Giakoumelis and Lam Sample C3

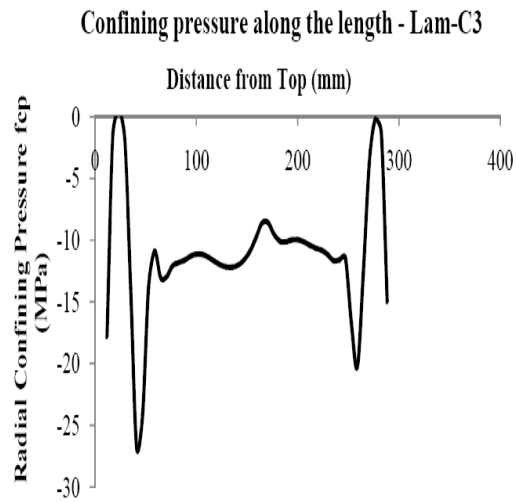

Figure 25: Variation of confining pressure along Giakoumelis and Lam Sample C3

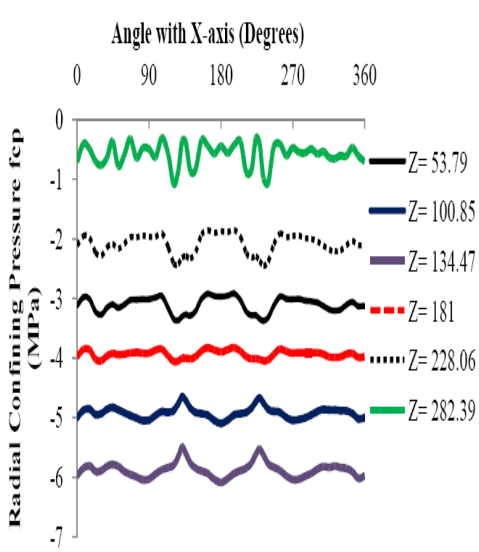

Figure 26: Radial confining pressure distribution the

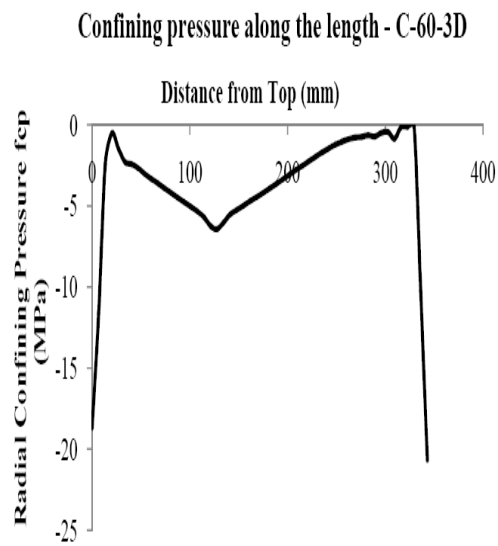

Figure 27: Variation of confining pressure along

at different sections along the height of Oliveira et al. Sample C-60-3D

height of Sample C-60-3D

Further, a comparison of this maximum confining pressure obtained from Abaqus (using Figs. 23, 25 and 27 within the middle end restraint free length) with the uniform confining pressure obtained from Huang et al. (2002) has been shown in Table 6.

Column	Source	D/t	Max. Confining Pr. From Numerical model $f_{cp\text{-}max}$ (MPa)	Confining Pr. From Huang et al [6] f_l (MPa)	$f_{cp\text{-}max}$ / f_l
C-60-3D	Oliveira et al	34.12	6.434	4.384	1.467
C-100-3D	Oliveira et al	34.12	12.174	4.384	2.776
C3	Giakoumelis and Lam	28.75	13.025	6.765	1.925
C14	Giakoumelis and Lam	29.82	18.682	6.468	2.880
CC4-A-4-1	Sakino et al	50.34	4.389	1.369	3.206
CC4-C-4-1	Sakino et al	101.35	4.354	0.732	5.940
D4M4F1	Gupta et al	38.95	7.821	1.746	4.480

Table 6: Comparison of max simulated vs theoretically obtained confining pressures

From the data, it is clear that the actual peak confining pressure across the height of the specimen can reach up to as much as 6 times the confining pressure predicted by Huang et al. This implies that it may be possible to load concrete up to a stress value higher than that predicted by Huang et al. (2002).

6 CONCLUSIONS

The paper presents a numerical model for the simulation of short concrete filled steel tubular columns loaded in axial compression using the commercial finite element code ABAQUS (ABAQUS 6.9, 2009). The simulation procedure attempts to model the confining effect of steel tube on concrete using a confined stress strain model for concrete available in literature. To judge the accuracy of the model, the output peak axial load bearing capacity and the deformed shape are compared to the corresponding values from the literature. It is observed that the proposed model can be used to predict the axial load capacity of stub steel tubular columns filled with concrete of compressive strength upto 100 MPa. The model is also able to capture the local buckling of steel tube, which is a common mode of failure of short CFST columns. After validation, the proposed model is used to study the variation of radial confining pressure in concrete along the circumference as well as along the height of the specimen. It is concluded that:

1 The overall load-deflection behaviour and the deformed shape of the CFST column remain unchanged irrespective of the end friction between the compression member and the beam (or platen) above it. Even for high end friction value of 0.5, negligible change in the result parameters was observed for short columns.

2 The change in effective length does not influence much the response of the stub CFST column under axial compression.
3 The confining pressure provided by the steel tube to concrete is largely exaggerated near the column ends by the friction between machine platen and CFST. The affected length of CFST column was generally between 30 mm and 50 mm from either side. This results in very high compressive stresses in concrete in these areas, thereby generally causing the initial local buckling to occur near the platens in the early stages of the loading. It is thus advised that instead of being misled by these values, the radial confining pressure (and hence concrete compressive strength) in the middle (end-restraint free) length should be used for any comparisons or design purposes
4 It is seen that even within the middle (end-friction free) region of the specimen, the confining pressure is not constant with the length. Instead, it follows a V-shaped distribution in this region, with the maximum value being reported near the region of local buckling or concrete bulging in this length.
5 The maximum confining pressure obtained from the Abaqus (ABAQUS 6.9, 2009) model is generally higher than the uniform value for the same predicted by Huang et al. (2002).
6 More studies are required to develop an exact model for confinement of concrete in CFST members, which takes into account the variation in confining pressure along the length of column as well.

References

ABAQUS 6.9 Documentation, ABAQUS Users and Analysis Users Manual 2009, Providence R.I.

Bahrami, A. , Badaruzzaman Wan HW. , Osman AS. Behaviour of stiffened concrete-filled steel composite (CFSC) stub columns. Latin American Journal of Solids and Structures 10(2):409-440.

Ellobody, E. et al (2006). Behaviour of normal and high strength concrete-filled compact steel tube circular stub columns. Journal of Constructional Steel Research 62:706-715.

Giakoumelis, G. and Lam, D. (2004). Axial capacity of circular concrete-filled tube columns. Journal of Constructional Steel Research 60(9): 1049-1068.

Gupta, P.K. and Gupta, N.K. (2005). Multiple barrelling in axial compression of cylindrical tubes. Latin American Journal of Solids and Structures 2:195-217.

Gupta, P.K. et al. (2007). Experimental and computational study of concrete filled steel tubular columns under axial loads. Journal of Constructional Steel Research 63: 182-193.

Huang, C. et al. (2002). Axial load behaviour of stiffened concrete-filled steel columns. Journal of Structural Engineering ASCE 128(9): 1222-30.

IS 456:2000 (Reaffirmed 2005), *Indian Standard* Code of Practice-Plain and Reinforced Concrete (*Fourth Revision*), Bureau of Indian Standards, India.

Johansson, M. and Gylltoft, K. (2001). Structural behaviour of slender circular steel-concrete composite columns under various means of load application. Steel and Composite Structures 1(4): 393-410.

Oliveira, WLA. et al. (2009). Influence of concrete strength and length/diameter on the axial capacity of CFT columns. Journal of Constructional Steel Research 65(12): 2103-2121.

O'Shea, MD. and Bridge, RQ. (2000).Design of circular thin-walled concrete filled steel tubes. Journal of Structural Engineering ASCE 126(11): 1295-1303.

Sakino, K. et al. (2004). Behaviour of Centrally Loaded Concrete-Filled Steel-Tube Short Columns. Journal of Structural Engineering ASCE 130(2): 180-88.

Shanmugam, NE. and Lakshmi, B. (2007). State of the art report on steel-concrete composite columns. Journal of Constructional Steel Research 57(10): 1041-1080.

Schneider, S.P. (1998). Axially loaded concrete-filled steel tubes. Journal of Structural Engineering ASCE 124(10): 1125-1138.

Tomii, M. ,Yoshimura, K., and Morishita, Y. (1977). Experimental studies on concrete filled steel tubular stub columns under concentric loading. Proceedings of the International Colloquium on Stability of Structures under Static and Dynamic Loads: 718-741.